Oxygen Evolution Catalysts under Proton Exchange Membrane Conditions in a Conventional Three Electrode Cell vs. Electrolyser Device: A Comparison Study and a 3D-Printed Electrolyser for Academic Labs

Michelle P. Browne[ab#], James Dodwell[c#], Filip Novotny[a], Sonia Jaśkaniec[b], Paul R. Shearing[c], Valeria Nicolosi[bd], Dan J.L. Brett[c] and Martin Pumera[aefg]

[#] joint first authorship

[a] Center for Advanced Functional Nanorobots, Department of Inorganic Chemistry, University of Chemistry and Technology Prague, Technicka 5, 166 28 Prague 6, Czech Republic
[b] Centre for Research on Adaptive Nanostructures and Nanodevices (CRANN), Advanced Materials and BioEngineering Research (AMBER) Centre and School of Chemistry, Trinity College Dublin, Ireland.
[c] Electrochemical Innovation Lab, Department of Chemical Engineering, University College London, London, WC1E 7JE, United Kingdom
[d] I-Form Research Center, Trinity College Dublin, Dublin, Ireland
[e] Department of Medical Research, China Medical University Hospital, China Medical University, No. 91 Hsueh-Shih Road, Taichung, Taiwan
[f] Department of Chemical and Biomolecular Engineering, Yonsei University, 50 Yonsei-ro, Seodaemun-gu, Seoul 03722, Korea
[g] Future Energy and Innovation Laboratory, Central European Institute of Technology, Brno University of Technology, Purkyňova 656/123, Brno, CZ-616 00, Czech Republic

Author for correspondence: M.Pumera, pumera.group@gmail.com

Keywords: OER; Electrolysers; Conventional three-electrode cell; Transition metal oxides; 3D-printing.

Abstract

Developing active and stable Oxygen Evolution Reaction (OER) catalysts that can operate in electrolyser environments is of utmost important in order to produce H_2 gas for electricity generation. Currently, many of these studies are carried out in conventional three-electrode cell set-ups; however, this configuration may not accurately represent conditions experienced under practical electrolyser conditions. Herein, a range of transition metal oxide (TMO) catalysts are evaluated and compared in a three-electrode cell and in an electrolyser. We show that the same catalyst significantly underperforms in a three-electrode cell. Hence, many OER catalysts in academic labs may have been erroneously omitted from further optimisation processes due to showing 'poor' performance in conventional three-electrode cells. Herein, we wish to show this discrepancy experimentally and suggest a solution to scientists wanting to find active OER catalysts by using 3D-printing to inexpensively manufacture electrolyser devices for OER catalyst evaluation.

1. Introduction

Electrolyser devices (including Proton Exchange Membrane (PEM) and Alkaline Exchange Membrane (AEM) electrolysers), powered by a renewable source of electricity, e.g. solar or wind, are attractive non-fossil fuel-based avenues for producing clean hydrogen which could be used in a fuel cell to make electricity for various industries and applications, including automotive.[1] It has been estimated that only 4% of the world's hydrogen is produced by water electrolysis,[2] as such, improving the performance of these technologies will see the utilisation of these devices increase dramatically.[2] In a water electrolyser, the aim is to produce H_2 gas on the cathode through the Hydrogen Evolution Reaction (HER).[3, 4] However, a major challenge in improving electrolyser performance is related to the large overpotentials associated to the Oxygen Evolution Reaction (OER) at the anode.[3, 5, 6]

Schmidt and co-workers predicted that PEM electrolysers will be the dominant technology for hydrogen production by the year 2030.[7] PEM electrolysers are advantageous over AEM electrolysers as the Raney Ni 'state-of-the-art' AEM catalysts underperforms compared to the IrO_2/Pt catalysts in a PEM device, especially at current densities over 200 mA cm^{-2}.[8] However, the majority of current academic research in the area of new catalysts for water splitting, in particularly for OER catalysts, is undertaken in alkaline conditions which is largely due to the fact that most inexpensive materials will corrode under OER conditions in acidic media.[9, 10] This contradiction between the future of electrolysis, based on PEMs, and alkaline electrolysis dominating the current water-splitting research landscape, could be partly due to new catalysts exhibiting inefficient activity and instability under the current evaluation conditions in a research lab setting.

Currently, most studies based on developing new materials for PEM electrolysis are conducted in conventional three-electrode cells, illustrated in **Figure 1A and Table 1**, with relatively small geometric areas and lower catalyst loadings compared to that used in practical electrolyser devices, illustrated in **Figure 1B and Table 1**.[11-15] In relation to the catalyst loading, as the loadings used for electrolyser devices are much higher than in a conventional three-electrode cell, the thicker catalyst coating results in only a portion of the material being accessible to the liquid electrolyte and participating in the

reaction at the catalyst surface. Furthermore, the higher catalyst loading in practical electrolysers allows for longer lifetimes due to a 'reserve' in catalyst compared to three-electrode cell testing. Additionally, the electrolyte, the electrode microstructure, and the temperature of the reaction differ significantly in literature when comparing catalysts for the OER in conventional three-electrode cell set-ups and in electrolyser devices, Table 1. Hence, there is a major discrepancy between the operational parameters of these two testing platforms, which leads to the question; Is the three-electrode cell set-up representative of practical electrolyser operation and an appropriate means of evaluating OER catalysts?

For other important electrochemical energy conversion reactions, such as the OER in alkaline media and the Oxygen Reduction Reaction (ORR) in acidic media, researchers have shown that conventional evaluation techniques are not necessarily suitable for catalyst screening for the desired application.[16-18] Boettcher and co-workers showed that for alkaline anion exchange-membrane (AAEM) water electrolysis, there is a significant difference in the OER performance of metal oxides/hydroxides in a three-electrode cell configuration and an AAEM water electrolyser.[17] Furthermore, to evaluate catalysts for the ORR in a fuel cell, Arenz and co-workers developed a gas diffusion electrode set-up which provides more realistic ORR performance results compared to the commonly used rotating disc electrode in a three-electrode cell set-up.[16] Therefore, the current evaluation process for the OER in acidic media must also be assessed to ensure robust and representative measurement in order to develop next generation catalytic materials for PEM electrolysers.

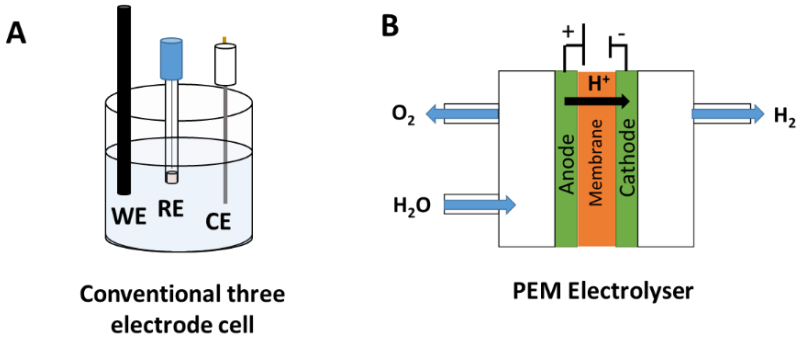

Figure 1. Conventional three-electrode cell set-up and electrolyser device set-up

Herein, a range of metal oxides were analysed as catalysts for the OER under acidic/PEM conditions in a conventional three-electrode cell (half-cell) and in an 3-electrode electrolyser device, in order to validate whether the three-electrode cell performance is a translatable method for the evaluation of OER catalysts for electrolyser devices. Transition metal oxides (TMO) were chosen in this study as it is well known that this class of materials are good candidates for the OER in acidic media and hence, are one of the most frequently studied materials for this reaction.[19-21] The results of this work indicate that the performance of the metal oxides in conventional three-electrode cells does not universally correlate with those measured in an electrolyser device. In order to provide a solution to this issue, low-cost electrolyser devices were produced using various additive manufacturing technologies (Fused Deposition Modelling (FDM) and Stereolithography (SLA)) in order to evaluate OER catalysts under more realistic PEM conditions.[22-24] Some of the 3D-printed electrolysers exhibit near-identical performance to a practical electrolyser and can be 3D-printed using low-cost and commercially available 3D-printers and precursor materials. These 3D-printed electrolysers provide a more realistic evaluation of OER catalysts than the conventional three-electrode cell configuration and so provides a more robust means of catalyst activity evaluation for the development of next-generation PEM electrolysers.

Table 1. Common measurement parameters for conventional three-electrode cell set-ups and electrolyser devices in relation to water splitting in acidic/PEM environments

	Three electrode cell	**Ref**	**Electrolyser device**	**Ref**
Electrolyte	0.5 M - 1 M aqueous H_2SO_4	21, 25, 26	Nafion membrane	27, 28
Ink	Mixture of Nafion, ethanol and water. (Nafion very low wt%).	19, 29	Mixture of Nafion, ethanol and water. (Nafion very high wt%).	30
Working Electrode	Low catalyst loadings in academic labs. Typical loading between 0.1 to 1 mg cm^{-2} Common support: Glassy Carbon	12, 21, 25, 31	High catalyst loadings in academic labs 3 mg cm^{-2} Common support: Catalyst Coated Membranes (CCMs): no support. Ink deposited straight onto the Nafion membrane. Large geometric areas of 5 cm^2 or more.	1, 27 28

	Small geometric area of ~ 0.1 cm^2			
Operational mode	Potentiostatic	[21, 26]	Galvanostatic	[32, 33]
Temperature	Usually room temperature		50 °C – 80 °C	[27, 28, 33]

2. Experimental Section

2.1 Synthesis of Adams' catalysts

The metal oxide catalysts were fabricated by a previously reported modified Adams' method.[34] In this study, 10 g of sodium nitrate and 0.5 g of the relevant metal salt were added to a porcelain crucible and dissolved in de-ionised water. Afterwards, the crucible was placed in a muffle furnace and the temperature of was ramped up to 500 °C (10 °C per minute) in air. The crucible was heated at 500 °C for 30 mins then allowed to cool down to room temperature. After the crucible had cooled, the product was cleaned with de-ionised water and centrifugation to remove the excess salt. The product was then dried in an oven at 100 °C. Finally, the structure of the metal oxide was determined by XRD with a D2 Phaser (Bruker) equipped with a Cu Kα source (λ = 1.5418 Å).

2.2 Conventional three-electrode cell working electrode preparation and measurements

The three-electrode cell measurements were conducted using an Autolab potentiostat with a commercial glassy carbon (GC) electrode as the working electrode, an Ag/AgCl reference electrode (1M KCl), and a carbon rod as the counter electrode. The electrolyte used was 0.5 M H_2SO_4. The metal oxides were drop-cast onto the rotating disc glassy carbon (GC) electrodes from a suspension containing the relevant metal oxide (10 mg ml^{-1}), 0.5 ml de-ionised water, 0.5 ml ethanol and 8µl Nafion; ink suspension components similar to those found for OER reports from in literature.[35, 36] The catalyst loading of the metal oxides onto the GC electrode was ~0.7 mg cm^{-2}, unless otherwise stated. A catalyst loading 0.7 mg cm^{-2} of is a typical averaged value used across literature for the evaluation

of OER catalysts in a conventional three electrode cell set-up.[31] The metal oxide modified rotating disc GC electrode was attached to a rotating disc electrode (RDE) set-up. The RDE measurements were all carried out using a rpm of 1600. The linear sweep voltammetry (LSV) measurements were carried out at a scan rate of 1 mV s^{-1} and were iR corrected. Electrochemical Impedance Spectroscopy (EIS) was carried out in the frequency range of 100000 to 0.1 Hz in a non-Faradic region. The chronopotentiometry measurements were carried out a current density of 10 mA cm^{-2}.

2.3 Catalyst Coated Membrane (CCM) preparation

To prepare a CCM for the electrolyser device measurements, 3 mg cm^{-2} of the relevant metal oxide and 0.5 mg cm^{-2} of Pt/C were spray-coated onto separate glass reinforced Teflon sheets (Sigma Aldrich) using a 5 cm^2 geometric area mask, Figure S6. The two catalyst coated Teflon sheets were sandwiched with a Nafion 117 membrane in the centre and hot-pressed at 140 ^oC at 2 MPa for 5 minutes. Before testing, the CCMs were immersed in 0.5 M H_2SO_4 for 12 hours.

2.4 Electrolyser device measurements – three electrode in the PEEK cell (Figure 4 and 5)

The PEM electrolyser device, with a geometric active area of 5 cm^2, used in the evaluation of the metal oxides was fabricated in house by machining polyetheretherketone (PEEK) (Sigma Aldrich) to create a bespoke electrolyser, as illustrated in Figure 2A.[37] To assemble the electrolyser, Pt-coated components consisting of a Ti piston, expanded Ti mesh (Deze titanium – 2 mm LWD 1 mm SWD) and Ti sinter (Merelex Corporation, TI-M-01-FM.2MMT - 100 µm average pore size) were inserted to the anode and cathode compartments. The pistons were needed to apply pressure to the cell and to connect the electrolyser to the potentiostat (Gamry Instruments). The mesh and sinters were used as electrical contacts and gas/water diffusion layers to the CCM. The CCM was then sandwiched between the two compartments and the two sections bolted together. In operation, 1.4 MPa pneumatic pressure is applied to the Ti pistons to create good electrical contact between the mesh, sinter and CCM. (See SI Table S1 for estimated cost of a piston, mesh and sinter).

Peristaltic pumps supplied de-ionised water into both sides of the cell from separate water tanks; the water was heated to 60 °C, with a flow rate of 25 ml min^{-1}, and kept at a constant temperature by a thermostat bath. A reference electrode was connected to the CCM by a 2 mm hole drilled through the sealing edge of the PEEK on the anode side, positioned 1 mm away from the CCM active area but contacting the CCM sealing edge. With the hole filled with 0.5 M sulfuric acid and connected to an electrolyte reservoir with a $Hg/HgSO_4$ reference electrode (0.5 M H_2SO_4), the CCM sealing edge acts as the remaining extension of the Luggin capillary to the electrodes. This setup, therefore, allows for the direct measurement of the OER potentials rather than the overall cell voltage.[37] The I-V curves were obtained by applying a stepwise sequence of current densities between 0.01 mA cm^{-2} and 1 A cm^{-2} and holding for 60 seconds each. The chronopotentiometry measurements were run at a constant current density of 10 mA cm^{-2}.

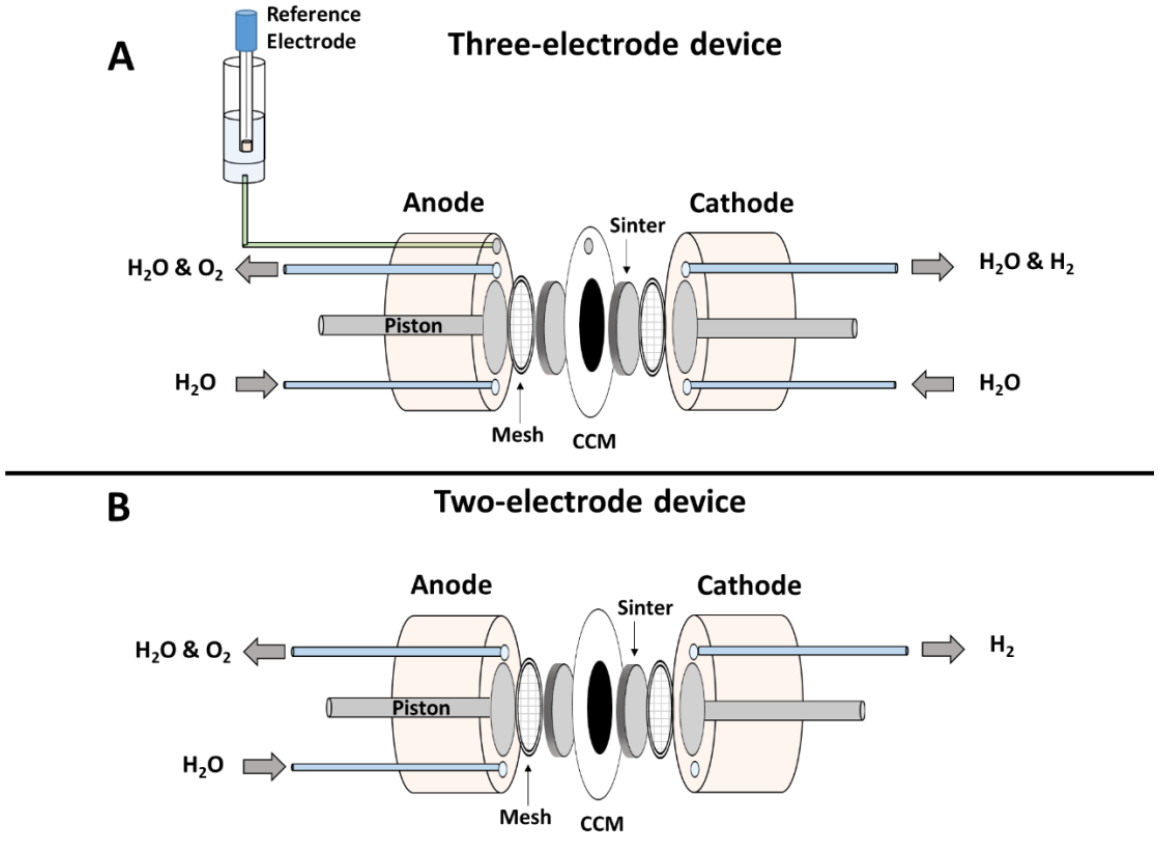

Figure 2A. Schematic of the PEEK electrolyser device (three-electrode cell) set-up used for the evaluation of the metal oxide materials in Figure 4 and 5 and **B.** Schematic of the 3D-printed electrolyser device (two-electrode cell) set-up used for the evaluation of the IrO_2/Pt CCM in Figure 6 and 7.

2.5 3D-Printing of the electrolyser devices

For the purpose of 3D printing, the cell model used for the manufacturing of the PEEK cell was modified to avoid overhangs in the structure which would need supports to print successfully. Fusion 360 (Autodesk) was used to perform this optimisation, the parametric 3D model was then exported into the .stl format for slicing in respective printer software. For the FDM 3D-printing, the .stl file was sliced using Slic3r (Prusa) open-source software with a common layer height of 0.2 mm, wall thickness of 3 perimeters (~1.2 mm) and 5% infill using a grid pattern. FDM 3D-printing was carried out using an i3 MK3s Prusa printer with a 0.4 mm nozzle. The printing temperature of the nozzle was 230 °C for PETG filament and 260 °C for the Co-polyester filament. The sliced model was exported to .gcode format for the actual printing. For the SLA 3D-printing, the .stl file was sliced using PreForm software (FormLab). The Layer height was set to 0.1 mm for all the SLA materials. The SLA 3D-printing was conducted with a Form 2 SLA printer (Formlabs).

2.6 Electrolyser device measurements – two-electrode in 3D-printed electrolysers (Figure 6 and 7)

For the two-electrode electrolyser measurements, the 3D-printed compartments with the CCM were assembled similar to the three electrode electrolyser shown in Figure 2A but without an integrated reference electrode as illustrated in Figure 2B. The electrolyser was operated with inlet water heated to 60 °C, with the flow rate set at 25 ml min^{-1}. The anode water flow came from an anode water tower, heated using a thermostat bath, and delivered to the cell using a peristaltic pump. The outlet was connected back to the anode tower. The cathode was run dry. The I-V curves and the chronoamperometry measurements were carried under the same current parameters as the three-electrode device measurements. The electrochemical impedance measurements were carried out in a frequency region of 50000 – 0.1 Hz at a potential of 0.3 V, to ensure no OER processes were occuring to determine the inherent cell ohmic losses.

3. Results and Discussion

3.1. Synthesis of transition metal oxide (TMO) catalysts

Five metal oxide catalysts were fabricated by the Adams methods from metal salts to test as OER catalysts in a conventional three-electrode cell and 3-electrode electrolyser device. The fabrication of the Adams' powder catalysts was carried out via the thermal decomposition of a metal salt, containing Ru, Co, Mn, Ni or Fe, with sodium nitrate in water, as described previously.[38] The five powder materials produced were characterised by X-Ray Diffraction (XRD) to determine the phase composition, shown in **Figure 3**. The powder synthesised from the metal salts containing Ru, Co, Mn, Ni and Fe were all successfully converted to metal oxides during the thermal annealing procedure.

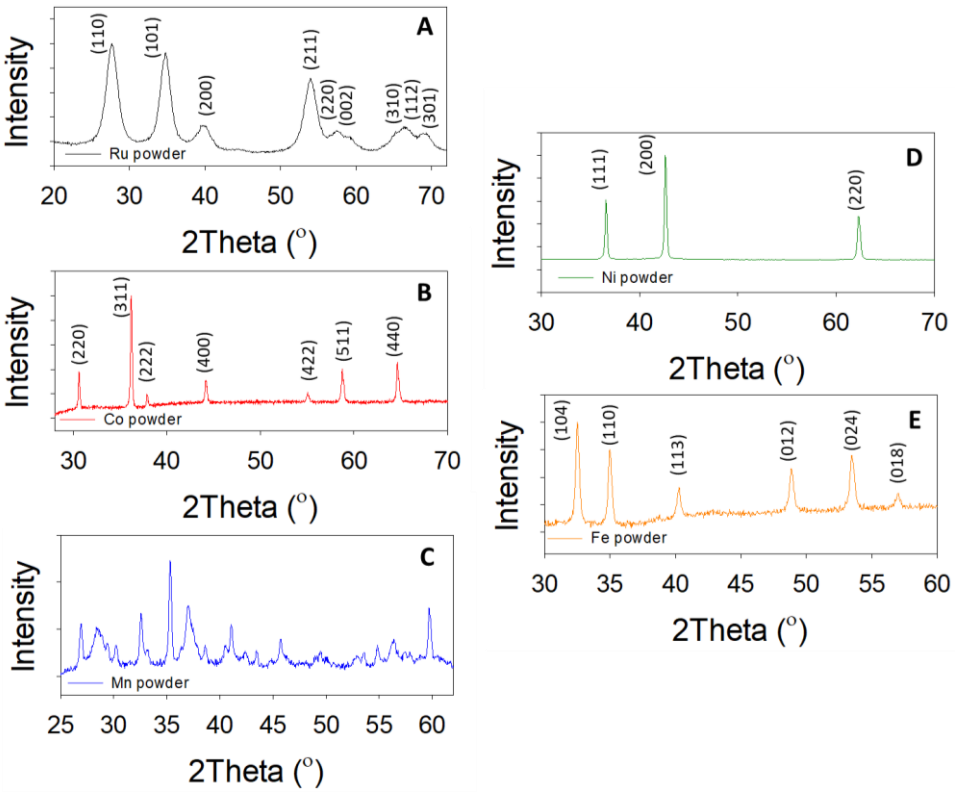

Figure 3. XRD patterns for the powder materials used for the three-electrode cell and device measurements fabricated from the Adams' Fusion Method: **A)** Ru Adams, **B)** Co Adams, **C)** Mn Adams, **D)** Ni Adams and **E)** Fe Adams.

The XRD pattern of the powder resulting from the Adams' method synthetic route using Ru metal salts can be indexed to RuO_2, **Figure 3A**.[39] This is confirmed by the presence of the reflective peaks at the 2θ values of 27.7°, 34.8°, 39.6°, 54.0°, 57.3°, 59.3°, 65.4°, 66.4° and 68.9° corresponding to the RuO_2

lattice planes of (110), (101), (200), (211), (220), (002), (310), (112) and (301), respectively. The Miller indices of (220), (311), (222), (400), (422), (511) and (440) for Co_3O_4 at the 2θ values of 30.7°, 36.3°, 37.9°, 44.1°, 55.1°, 58.8° and 64.6°, respectively, are present for the thermally annealed Co metal salt based powder, **Figure 3B**.[40] The Mn oxide synthesised contained XRD peaks corresponding to a variety of manganese oxides including Mn_2O_3 and Mn_3O_4, **Figure 3C**.[41] Due to the complexity of the Mn oxide powder, this material will be designated as MnO_x for this study. The powder resulting from the Ni metal salt can be indexed to NiO due to the presence of the reflective peaks at 36.6°, 42.8° and 62.4°, corresponding to the crystal planes of (111), (200) and (220), respectively, **Figure 3D**.[42] Finally, the Fe salt based reactants converted into α-Fe_2O_3. This was evident due to the detection of the peaks at 32.4°, 35.0°, 40.2°, 48.9°, 53.5° and 57.0° that correspond to the α-Fe_2O_3 crystal planes of (104), (110), (113), (012), (024) and (018), respectively, **Figure 3E**.

3.2. Comparison of the conventional three-electrode cell vs. electrolyser device using synthesised the TMO materials for OER evaluation under common conditions.

The water oxidation experiments of the TMO catalysts were carried out in a three-electrode cell and in an electrolyser device, under common conditions found in the literature for each platform (based on Table 1), to determine if the two techniques are complementary; i.e. if the three-electrode set-up is a good indicator of how catalysts perform under representative electrolyser conditions, as shown in **Figure 4**.

As conventional three-electrode cell measurements are carried out using a reference electrode in order to isolate the electrode reaction of interest (the working electrode),[3] the electrolyser device used for these comparative studies was modified to allow for a reference electrode to be a part of the device design,[37, 43] as shown in **Figure 2A**.

The linear sweep voltammetry (LSV) curves for the in-house synthesised RuO_2, Co_3O_4, MnO_x, NiO and Fe_2O_3 in a conventional three-electrode cell are illustrated in **Figure 4A and Figure S3-7**. It is clear that the RuO_2 is the optimum catalyst under the acidic three-electrode cell conditions compared to the

other transition metal oxides, as it exhibits a potential of ca. 1.6 V vs RHE at a current density of 10 mA cm^{-2}, which is a common result in literature for RuO_2 under acidic conditions.[21] The extremely low activity of the first row TMOs (Co_3O_4, MnO_x, NiO and Fe_2O_3) in the 0.5 M H_2SO_4 electrolyte could be due to the degradation of these materials in the acidic corrosive environment under the applied OER potentials, which is common for these earth abundant based materials.[44]

Next, the in-house catalysts were evaluated using standard protocols under PEM electrolyser conditions; i.e. current – potential (I-V) curves, shown in **Figure 4B** (the y- and x-axes of the I-V curves are plotted inversely to allow for comparison with the LSV curves). Interestingly, when each of the in-house transition metal oxide (TMO) catalysts are constructed into a CCM, inserted into the electrolyser device and benchmarked under the same conditions, all of the catalysts (RuO_2, Co_3O_4, MnO_x, NiO and Fe_2O_3) seem to exhibit much-improved OER activity than when evaluated in the three-electrode cell.

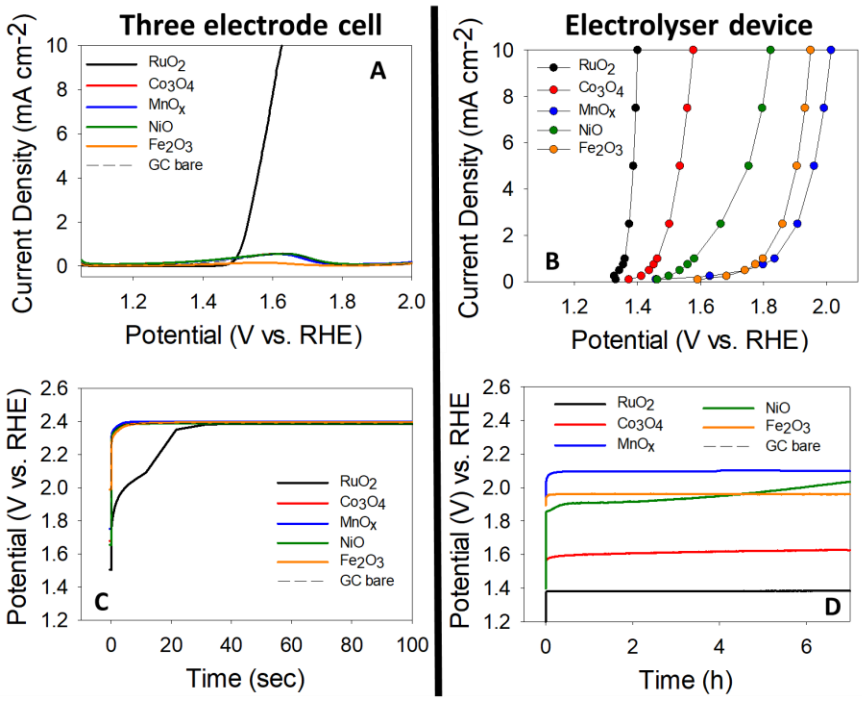

Figure 4. Three-electrode cell vs. electrolyser device (with integrated reference electrode) measurements under acidic conditions for range of TMO catalysts. **A)** Linear sweep voltammetry (iR-corrected) in a three-electrode cell configuration at a scan rate of 1 mV s^{-1} in 0.5 M H_2SO_4 at an rpm of 1600. **B)** I-V curves in a PEM device using a Nafion membrane. **C)** Chronopotentiometry measurements in a three-electrode cell configuration at a current density of 10 mA cm^{-2} in 0.5 M H_2SO_4 at an rpm of 1600 and **D)** Chronopotentiometry measurements in a PEM device using a Nafion membrane at a current density of 10 mA cm^{-2}. **Note:** All of the electrolyser measurements in Figure 4 B and D are conducted using the PEEK electrolyser cell with the integrated reference electrode illustrated in Figure 6A.

Indeed, the best performing catalyst is again the RuO_2. However in the PEM device, the Co_3O_4, NiO and Fe_2O_3 catalysts all reach a current density of 10 mA cm^{-2} at or before 2 V vs. RHE, while the MnO_x reaches a current density of 8 mA cm^{-2} at this potential; this is contrary to the corresponding result from the three-electrode cell set-up where none of the earth abundant materials even reach a current density of 1 mA cm^{-2}.

As the durability of OER catalysts is another extremely important parameter that must be assessed during OER evaluation, the TMO catalysts underwent longevity testing under electrochemical conditions routinely applied in the literature using the conventional three-electrode cell; i.e. monitoring of the potential at a constant applied current density of 10 mA cm^{-2} over a period of time.[10, 45] Again, to determine the compatibility of the three-electrode cell results with those of the electrolyser device, all of the materials underwent stability tests under both set-ups at a current density of 10 mA cm^{-2}. From **Figure 4C**, the chronopotentiometry curves of the Co_3O_4, MnO_x, NiO and Fe_2O_3 materials in the conventional three-electrode cell all exhibit similar potentials (V vs. RHE) as the GC substrate, indicating that these cheap TMO materials have either become in-active or degraded under the applied OER environment. The RuO_2 on the GC substrate shows a continuously declining performance until it also reaches the same potential as the GC substrate at a time of ~40 s. On the other hand, in the electrolyser device, illustrated in **Figure 4D**, the RuO_2, Co_3O_4, MnO_x, and Fe_2O_3 materials are all stable over a period of 6 hours, while the NiO catalysts begin to decline after 2 hours. This clearly shows that the three-electrode cell configuration is a poor indicator of the stability of a catalyst for the OER in an electrolyser device.

3.3 Why is there a difference in the activity and stability between the conventional three electrode cell and the electrolyser three electrode device?

From a comparison of the LSV/I-V curves and the chronopotentiometry from the three-electrode set-up, Figure 4 A and C respectively, and the electrolyser device set-up, Figure 4B and D respectively, it is clear that the three-electrode cell set-up currently undertaken throughout the literature in academic

labs is not a sufficient method for the evaluation of transition metal catalysts for PEM electrolyser devices. The results obtained during the OER evaluation measurements in the conventional three electrode cell could potentially result in the omission of these materials from further investigation however, in the electrolyser device the same materials show promising activity. One must remember that the conventional three electrode cell platform is the most common evaluation method proposed in literature to benchmark materials for a water splitting therefore should give a reasonable indication of the activity and stability in a electrolyser device; as the electrolyser device is the final application.[10] The reasoning behind the discrepancy in the activity and stability of the materials between the two platforms, outlined in Figure 4, may be rationalised between the difference in the parameters, e.g. catalyst loadings, electrolyte used and working electrode supports, utilised for the three-electrode cell set-up and the electrolyser device, outlined from literature in Table 1.

In a bid to determine if the variation in the catalyst loadings used in literature is the cause of the loss in the activity and stability of OER catalysts in the three electrode cell set-up when compared to the electrolyser device, LSV and chronopotentiometry measurements were carried out in the three electrode cell set-up, Figure 1A, with the RuO_2 catalyst (best-performing catalyst in Figure 4) with a catalyst loading of 3 mg cm^{-2} i.e. the same loading of the RuO_2 in the electrolyser device in this work, **Figure 5**.

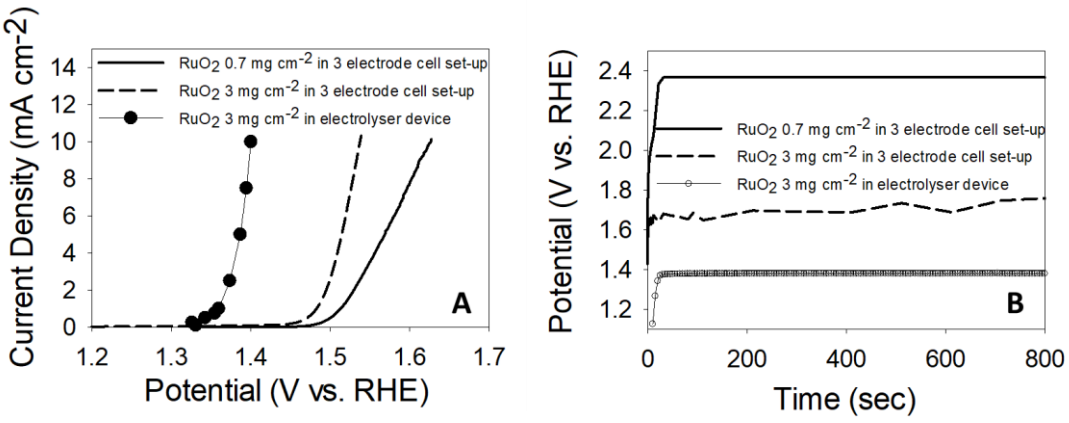

Figure 5 A. LSV curves of RuO_2 in a RDE three electrode set-up and an electrolyser device with various catalyst loadings and **B.** LSV curves of RuO_2 in a RDE three electrode set-up and an electrolyser device with various catalyst loadings

By comparing the LSV/I-V curves in **Figure 5A**, of the higher catalyst loading (3 mg cm^{-2}) on the RDE electrode in the three electrode cell set-up when compared to the lower catalyst loading (0.7 mg cm^{-2}) in the same set-up, it can be stated that the OER activity has improved. However, when compared to the same material (RuO_2 at a catalyst loading of 3 mg cm^{-2}) in the electrolyser device, the RuO_2 with the higher catalysts loading in the RDE still significantly under performs. Therefore, even if the catalyst loading of OER materials under investigation in RDE three electrode cells were the same as those utilised to make CCMs in electrolysers, the true activity of the catalysts for electrolyser applications would not be realised.

In terms of stability, the stability of the RuO_2 is improved with the higher mass loading in the RDE three electrode set-up compared to the RuO_2 with a catalyst loading of 0.7 mg cm^{-2}, **Figure 5B**. In fact, the RuO_2 in the RDE set-up with the lower catalyst loading seems to reach the same potential as the bare GC electrode in a matter of seconds during the chronopotentiometry measurement, Figure 4D. This is not the case for the RuO_2 with a catalyst loading of 3 mg cm^{-2}. The reasoning for the RuO_2 lower catalyst loading exhibiting extremely poor stability in acidic media may be due to the bare GC support undergoing passivation which essentially blocks the active material from being measured due to the increase in the contact resistance, which has been extensively studied by Cherevko and co-workers.[46] In the RDE set-up, with the RuO_2 at a higher catalyst loading this passivation effect of the GC electrode may not occur or occurs at a less significant rate which allows for the OER performance to be measured. Unfortunately, similar to the OER activity, the RuO_2 with a catalyst loading of 3 mg cm^{-2} in the RDE three electrode set-up under performs when compared to the same material on a CCM in the electrolyser, Figure 5B. This result suggests that the GC support used in the RDE three electrode cell may somewhat hinder the OER stability measurements.

Hence, it can be stated that the most common catalyst loadings (i.e. 0.1 to 1 mg cm^{-2}) and supports (GC electrodes) utilised in literature for OER evaluation in RDE three electrode cells plays a role in the discrepancy in the activity and stability when compared to the performance of the same materials in

an electrolyser but cannot explain the entire difference. The contact resistance in the two platforms is also likely to contribute to the increased activity and stability of the same material with the same catalyst loading in the electrolyser device, as the electrolyser device has an extremely low contact resistance due to the cell design when compared to the conventional three electrode set-up.

3.4. Development of 3D-printed electrolysers for the cheap evaluation of catalysts for the OER in acedemic labs

As the evaluation of both the activity and the stability of the materials in the conventional three-electrode set-up is clearly not a good indicator of device performance, there is the need for a cheap lab-deployable device capable of catalyst evaluation under more representative test conditions for PEM OER. As catalyst evaluation typically requires a high volume of discrete testing and tests over extended periods, a low-cost, in-house manufacturable solution is desirable. Herein, 3D-printing using various methods has been investigated to identify the most appropriate practical solution to manufacture an electrolyser device capable of screening PEM OER catalysts.

In order to show the diversity in the range of commercial 3D-printing filaments and low-cost 3D-printers which can be utilised to produce durable 3D-printed electrolyser devices for the evaluation of OER catalysts, four device assemblies were 3D-printed and the activity of a IrO_2/Pt CCM was compared to the practical PEM electrolyser with the intregrated reference electrode (made from PEEK), **Figure 6A**. **Note:** the IrO_2 and Pt are commercial materials and are know as the benchmark materials for PEM OER.[47]

Two of the electrolysers were 3D-printed using fused deposition modelling (FDM); one electrolyser using a glycol-modified polyethylene terephthalate (PET) filament, as shown in **Figure 6B**, and the other using a co-polyester filament (Co-P), as shown in **Figure 6C**.

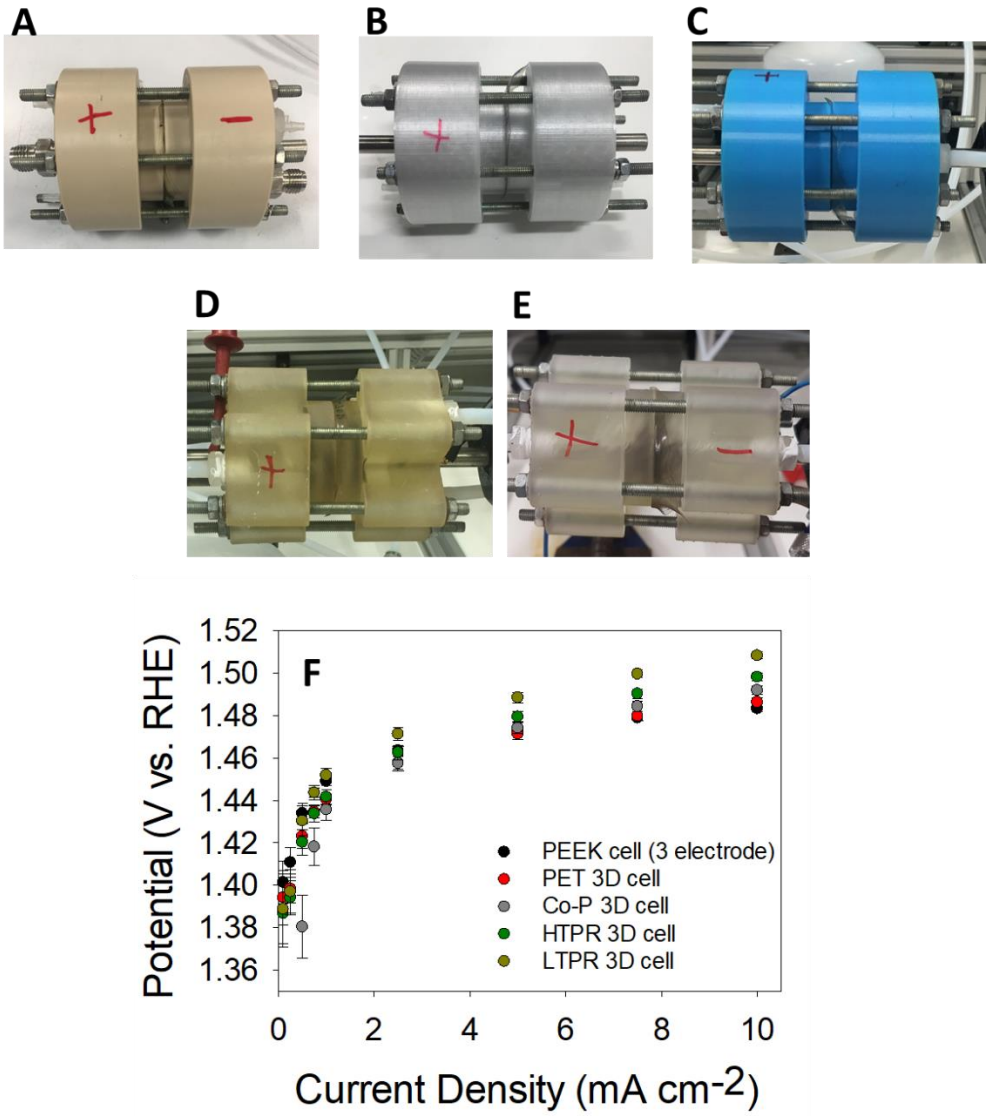

Figure 6. Comparison of the practical cell with the 3D-printed cells using a CCM fabricated using commercial IrO_2 and Pt/C. Photos of **(A)** PEEK, **(B)** PET, **(C)** co-polyester, **(D)** HTPR, **(E)** LTPR, and **(F)** I-V curves for these electrolyser assemblies.

The other two 3D-printed electrolysers were manufactured with stereolithography (SLA) using commercially available High-Temperature Photo Resin (HTPR), as illustrated in **Figure 6D**, and the other electrolyser with a Low-Temperature Photo Resin (LTPR), as shown in **Figure 6E**. (The design of the 3D-printed compartment used to construct the overall PEM cell device can be observed in **Figure S8**.)

The suitability of the 3D-printed electrolyser for OER catalysts evaluation was investigated under a two-electrode regime, shown in **Figure S9**, where the current/voltage response is that of the whole cell, to allow for a simple design for the 3D-printed electrodes. When using Pt as a catalyst for the

cathodic reaction for water splitting in an electrolyser device, the overpotential associated with the HER is negligible at low current densities (i.e. 10 mA cm^{-2}).[48] Therefore, in a two-electrode cell electrolyser device, the measured overpotential for the 'whole' cell can be mostly related to the potential for the OER/anodic reaction, See Figure S9 for more details. Before any water splitting measurements are conducted, the cell resistance must be tested.

Evaluation of the IrO_2/Pt CCM was carried out in the four two-electrode 3D-printed electrolysers (PET, Co-P, HTPR and LTPR) and in the three-electrode practical electrolyser (PEEK cell) to determine the optimum 3D-printing technique and precursor material for the fabrication of the 3D-printed electrolyser device. As observed in **Figure 6F**, the I-V curves show that all of the 3D-printed cells are capable of efficiently measuring the OER activity of the IrO_2/Pt CCM when compared to the I-V curve of the PEEK cell (practical three-electrode electrolyser). The inherent cell ohmic resistances of the 3D-printed cells are similar to the PEEK cell (ran in a two-electrode regime), as seen in the Nyquist plot in **Figure S10**. The ohmic values for the cell are 0.058, 0.067, 0.096, 0.101 and 0.103 Ω for the PEEK, PET, Co-P, HTPR and LTPR cells, respectively. Since, the same operating parameters for all the cells (e.g. the IrO_2/Pt CCM, temperature) are used, the ohmic resistance will give us the most information about how to improve the cell design/ indicate the best materials for the 3D-printed electrolysers. This is because the ohmic losses are due to the drop in the resistance due to the cell components i.e. the polymer material used to produce the 3D-printed cells; the only variable for these cells.[49] The increase in the ohmic resistances, which may contribute to the slightly higher activity observed for the Co-P, HTPR and LTPR cell when compared to the PET cell, may be due to the contact of the cell, pistons, meshes and sinters and the CCM which slightly changes with the material used for the fabrication of the 3D-printed cells.'

The stability tests of the IrO_2/Pt CCM in the PEEK and 3D-printed cells were conducted over a period of 6 hours at a current density of 10 mA cm^{-2} and are illustrated in **Figure 7A**. The PET and the Co-P cell are stable throughout the tests but the potential of the HTPR and LTPR based devices increases with time. The devices that show degradation with time are 3D-printed using photoresins; these are

known to be brittle and have low heat deflection temperatures (higher heat deflection temperature means a higher resistance to heat-induced defects/changes) due to the photoresin precursor materials. In this study, the electrolyte is maintained at a temperature of 60 °C which may cause the SLA 3D-printed electrolysers to be more susceptible to changes in the electrolyser structure over time, which could be responsible for the observed degradation in performance.[49, 50] Furthermore, some of the photoresin materials may leach from the cell body and influence the OER activity by depositing on the catalyst surface.

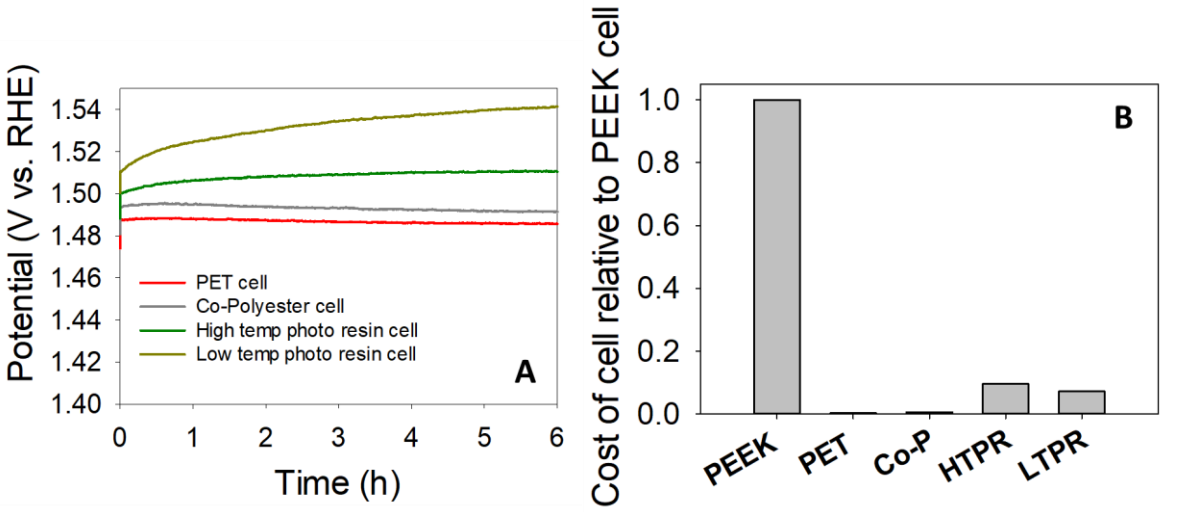

Figure 7A. Chronopotentiometry measurements in a two-electrode cell configuration for the 3D-printed electrolysers with the IrO_2 and Pt/C CCM and **B.** Cost analysis of the 3D-printed cells relative to the PEEK cell.

Finally, a cost evaluation analysis was carried out to compare the relative price of the 3D-printed electrolyser parts to the PEEK electrolyser parts used to construct the PEM cell. As shown in **Figure 7B**, all the 3D-printed electrolysers are less expensive to manufacture compared to the PEEK cell. Furthermore, the PETG cell, which shows similar performance to the PEEK cell for the evaluation of the CCM, is significantly less expensive than commercially available electrolysers that have the same active area of 5 cm^2, Table S2. Finally, the optimum combined 3D-printing technique and precursor materials to use to produce these devices would be FDM 3D-printing and the PETG filament due to the good stability of the IrO_2/Pt CCM in this device and the low cost of the PETG filament, respectively.

4. Conclusion

In summary, this work has shown that the conventional three-electrode cell set-up is not necessarily a good indicator of the activity and stability of catalysts for the OER in PEM electrolysers, particularly at low current densities of 10 mA cm^{-2}, which is the standard benchmark current density used in the literature. This is a serious concern, as most of the research into new catalysts for the OER are carried out using conventional three-electrode cells. Consequently, many TMO catalysts for the OER could have been omitted from further study as falsely deemed 'inactive' in a conventional three-electrode cell, when they may have shown promising performance in practical electrolyser devices using actual CCMs. As such, when screening candidate materials for electrolyser catalysts, it is imperative that these materials be tested in device configurations as well as the RDE conventional three elctrode cell set-up.

The difference in the activity and stability between the RDE three electrode cell and the electrolyser device, ran at common parameter found in literature, could somewhat be explained by a difference in catalysts loading and supports utilised however, cell design is also thought to play a role. As a solution to this issue and to access the true OER activity and stability of materials, the materials need to also be evaluated in a practical electrolyser device.

In order to address the issue of accessibility to test electrolyser devices in academic labs, we demonstrate that 3D-printed electrolyser cells can be fabricated using low-cost 3D-printers and commercially available precursors. These 3D-printed electrolyser cells were utilised to successfully evaluate CCMs with geometric surface areas relevant to a practical device. The results show that FDM 3D-printing using a PETG filament is the optimum 3D-printing technique and filament. Electrolyser devices produced by SLM and the photoresin precursors exhibited issues during the stability tests which can be related to the heat deflection temperature of the photoresin. Finally, a cost evaluation analysis of the 3D-printed devices revealed that the PET electrolyser was the least expensive device.

Finally, it is recommended that research groups utilise practical electrolyser devices in their OER research and not rely exclusively on conventional three-electrode cells. We are happy to share our CAD file for the 3D-printed electrolyser with researchers who are interested.

Conflicts of Interest

There are no conflicts to declare

Acknowledgements

M.P.B. would like to acknowledge the European Union's Horizon 2020 research and innovation programme under the Marie Skłodowska-Curie grant agreement No. 884318 (TriCat4Energy), the European Structural and Investment Funds OP RDE-funded project "ChemJets" (No. CZ.02.2.69/ 0.0/0.0/16_027/0008351) and the Royal Society of Chemistry (RSC) Researchers Mobility grant (no. RM1802-5340). P.R.S. acknowledges the support of The Royal Academy of Engineering (CiET1718/59). V.N acknowledges the support of SFI AMBER (12/RC/2278_P2) and the ERC CoG 3D2DPrint (681544). D.J.L.B would like to acknowledge funding from the EPSRC (EP/L015277/1, EP/P009050/1, EP/M014371/1, EP/M009394/1, EP/M023508/1, EP/L015749/1, EP/N022971/1) for supporting the hydrogen research in the Electrochemical Innovation Lab (EIL). M.P. acknowledges the financial support of Grant Agency of the Czech Republic (EXPRO: 19-26896X).

References

1. M. Carmo, D. L. Fritz, J. Mergel and D. Stolten, *Int. J. Hydrog. Energy*, 2013, **38**, 4901-4934.
2. S. Shiva Kumar and V. Himabindu, *Mater. Sci. Technol.*, 2019, **2**, 442-454.
3. C. Wei, R. R. Rao, J. Peng, B. Huang, I. E. L. Stephens, M. Risch, Z. J. Xu and Y. Shao-Horn, *Adv. Mater.*, 2019, **31**, 1806296.
4. X. Chia and M. Pumera, *Nature Catal.*, 2018, **1**, 909-921.
5. R. L. Doyle, I. J. Godwin, M. P. Brandon and M. E. G. Lyons, *Phys. Chem. Chem. Phys.*, 2013, **15**, 13737-13783.
6. F. Song, L. Bai, A. Moysiadou, S. Lee, C. Hu, L. Liardet and X. Hu, *J. Amer. Chem. Soc.*, 2018, **140**, 7748-7759.
7. O. Schmidt, A. Gambhir, I. Staffell, A. Hawkes, J. Nelson and S. Few, *Int. J. Hydrog. Energy*, 2017, **42**, 30470-30492.
8. K. E. Ayers, E. B. Anderson, C. Capuano, B. Carter, L. Dalton, G. Hanlon, J. Manco and M. Niedzwiecki, *ECS Trans.*, 2010, **33**, 3-15.
9. C. Hu, L. Zhang and J. Gong, *Energy Environ. Sci.*, 2019, **12**, 2620-2645.

10. C. C. L. McCrory, S. Jung, I. M. Ferrer, S. M. Chatman, J. C. Peters and T. F. Jaramillo, *J. Amer. Chem. Soc.*, 2015, **137**, 4347-4357.
11. R. Gusmão, Z. Sofer, J. Luxa and M. Pumera, *ACS Sustain. Chem. Eng.* 2019, **7**, 15790-15798.
12. C. L. Manzanares Palenzuela, J. Luxa, Z. Sofer and M. Pumera, *ACS Appl. Mater. Interfaces*, 2018, **10**, 17820-17826.
13. A. Ambrosi, Z. Sofer and M. Pumera, *Chem. Commun.*, 2015, **51**, 8450-8453.
14. A. B. Jorge, I. Dedigama, T. S. Miller, P. Shearing, D. J. L. Brett and P. F. McMillan, *Nanomaterials*, 2018, **8**, 16.
15. N. Mansor, T. S. Miller, I. Dedigama, A. B. Jorge, J. Jia, V. Brázdová, C. Mattevi, C. Gibbs, D. Hodgson, P. R. Shearing, C. A. Howard, F. Corà, M. Shaffer, D. J. L. Brett and P. F. McMillan, *Electrochim. Acta*, 2016, **222**, 44-57.
16. M. Inaba, A. W. Jensen, G. W. Sievers, M. Escudero-Escribano, A. Zana and M. Arenz, *Energy Environ. Sci.*, 2018, **11**, 988-994.
17. D. Xu, M. B. Stevens, M. R. Cosby, S. Z. Oener, A. M. Smith, L. J. Enman, K. E. Ayers, C. B. Capuano, J. N. Renner, N. Danilovic, Y. Li, H. Wang, Q. Zhang and S. W. Boettcher, *ACS Catal.*, 2019, **9**, 7-15.
18. H. Nolan and M. P. Browne, *Curr. Opin. Electrochem.*, 2020, **21**, 55-61.
19. P. P. Patel, M. K. Datta, O. I. Velikokhatnyi, R. Kuruba, K. Damodaran, P. Jampani, B. Gattu, P. M. Shanthi, S. S. Damle and P. N. Kumta, *Sci. Rep.*, 2016, **6**, 28367.
20. M. Etzi Coller Pascuzzi, A. Goryachev, J. P. Hofmann and E. J. M. Hensen, *Appl. Catal. B*, 2020, **261**, 118225.
21. Y. Lin, Z. Tian, L. Zhang, J. Ma, Z. Jiang, B. J. Deibert, R. Ge and L. Chen, *Nat. Commun.*, 2019, **10**, 162.
22. M. P. Browne, E. Redondo and M. Pumera, *Chem. Rev.*, 2020, **120**, 2783-2810.
23. A. Ambrosi and M. Pumera, *Chem. Soc. Rev.*, 2016, **45**, 2740-2755.
24. M. P. Browne, V. Urbanova, J. Plutnar, F. Novotný and M. Pumera, *J. Mater. Chem. A*, 2020, **8**, 1120-1126.
25. L. Yang, G. Yu, X. Ai, W. Yan, H. Duan, W. Chen, X. Li, T. Wang, C. Zhang, X. Huang, J.-S. Chen and X. Zou, *Nat. Commun.*, 2018, **9**, 5236.
26. P. E. Pearce, C. Yang, A. Iadecola, J. Rodriguez-Carvajal, G. Rousse, R. Dedryvère, A. M. Abakumov, D. Giaume, M. Deschamps, J.-M. Tarascon and A. Grimaud, *Chem. Mater.*, 2019, **31**, 5845-5855.
27. M. Maier, Q. Meyer, J. Majasan, C. Tan, I. Dedigama, J. Robinson, J. Dodwell, Y. Wu, L. Castanheira, G. Hinds, P. R. Shearing and D. J. L. Brett, *J. Power Sources*, 2019, **424**, 138-149.
28. G. Yang, S. Yu, Z. Kang, Y. Dohrmann, G. Bender, B. S. Pivovar, J. B. Green, Jr., S. T. Retterer, D. A. Cullen and F. Y. Zhang, *Energy Convers. Manag.*, 2019, DOI: 10.1016/j.enconman.2018.12.046, 108-116.
29. J. A. Arminio-Ravelo, A. W. Jensen, K. D. Jensen, J. Quinson and M. Escudero-Escribano, *ChemPhysChem*, 2019, **20**, 2956-2963.
30. M. Bernt, A. Siebel and H. A. Gasteiger, *J. Electrochem. Soc*, 2018, **165**, F305-F314.
31. A. A. S. Rovetta, M. P. Browne, A. Harvey, I. J. Godwin, J. N. Coleman and M. E. G. Lyons, *Nanotechnology*, 2017, **28**, 375401.
32. A. S. Gago, J. Bürkle, P. Lettenmeier, T. Morawietz, M. Handl, R. Hiesgen, F. Burggraf, P. A. Valles Beltran and K. A. Friedrich, *ECS Trans.*, 2018, **86**, 695-700.
33. M. Suermann, A. Pătru, T. J. Schmidt and F. N. Büchi, *Int. J. Hydrog. Energy*, 2017, **42**, 12076-12086.
34. E. Oakton, D. Lebedev, M. Povia, D. F. Abbott, E. Fabbri, A. Fedorov, M. Nachtegaal, C. Copéret and T. J. Schmidt, *ACS Catal.*, 2017, **7**, 2346-2352.
35. S. Jung, C. C. L. McCrory, I. M. Ferrer, J. C. Peters and T. F. Jaramillo, *J. Mater. Chem. A*, 2016, **4**, 3068-3076.
36. M. P. Browne and A. Mills, *J. Mater. Chem. A*, 2018, **6**, 14162-14169.

37. E. Brightman, J. Dodwell, N. van Dijk and G. Hinds, *Electrochem. Commun.*, 2015, **52**, 1-4.
38. M. P. Browne, C. O'Rourke, N. Wells and A. Mills, *ChemPhotoChem*, 2018, **2**, 293-299.
39. A. Ananth, M. S. Gandhi and Y. S. Mok, *J. Phys. D Appl. Phys.*, 2013, **46**, 155202.
40. D. D. M. Prabaharan, K. Sadaiyandi, M. Mahendran and S. Sagadevan, *Appl. Phys. A*, 2017, **123**.
41. A. Ramírez, P. Hillebrand, D. Stellmach, M. M. May, P. Bogdanoff and S. Fiechter, *J. Phys. Chem. C*, 2014, **118**, 14073-14081.
42. H. Yan, D. Zhang, J. Xu, Y. Lu, Y. Liu, K. Qiu, Y. Zhang and Y. Luo, *Nanoscale Res. Lett.*, 2014, **9**, 424.
43. H. Becker, L. Castanheira and G. Hinds, *J. Power Sources*, 2020, **448**, 227563.
44. W. Li, D. Xiong, X. Gao and L. Liu, *Chem. Commun.*, 2019, **55**, 8744-8763.
45. A. L. Strickler, D. Higgins and T. F. Jaramillo, *ACS Appl. Energy Mater.*, 2019, **2**, 5490-5498.
46. S. Geiger, O. Kasian, A. M. Mingers, S. S. Nicley, K. Haenen, K. J. J. Mayrhofer and S. Cherevko, *ChemSusChem*, 2017, **10**, 4140-4143.
47. A. W. Jensen, G. W. Sievers, K. D. Jensen, J. Quinson, J. A. Arminio-Ravelo, V. Brüser, M. Arenz and M. Escudero-Escribano, *J. Mater. Chem. A*, 2020, **8**, 1066-1071.
48. K. Ayers, *Curr. Opin. Electrochem.*, 2019, **18**, 9-15.
49. G. Chisholm, P. J. Kitson, N. D. Kirkaldy, L. G. Bloor and L. Cronin, *Energy Environ. Sci.*, 2014, **7**, 3026-3032.
50. Formlabs, Material Data Sheet Standard, https://dental-media.formlabs.com/datasheets/Standard-DataSheet.pdf).
51. Formlabs, Material Data Sheet High Temp, https://archive-media.formlabs.com/upload/HighTemp-DataSheet.pdf).